

Amplifying quantum correlations with quench dynamics in a quantum spin chain: Steady-states versus ground-states

Sasan Kheiri and Saeed Mahdavifar*

Department of Physics, University of Guilan, 41335-1914, Rasht, Iran

Hadi Cheraghi†

Institute of Physics, M. Curie-Skłodowska University, 20-031 Lublin, Poland

(Dated: April 21, 2022)

We analyze the behavior of steady-state quantum correlations (QCs) in the spin-1/2 transverse field XY chains analytically, in terms of quench dynamics at zero-temperature. We show that steady-state QCs are strikingly greater than the equilibrium ones in its ground-state, where a single quench is performed from ferro- into paramagnetic phases. Another framework to amplify the QCs here is a feasible protocol called double quench dynamics. To fulfill this purpose, we probe a middle quench point and spending time T (defined as the time passing from the middle quench point before reaching a second quench). By doing so, both single and double quenches act as practical tools to control the enhancement of the steady-state QCs in the final quenched point. In particular, and in parallel to expectations for some other quantities, we indicate that the nonequilibrium quantum phase transitions also can be identified by nonanalyticities in the steady-state QCs. Our work may be testable with the current class of trapped-ion or ultracold-atom experiments, and encourage the possible potential in the quantum information field.

PACS numbers:

I. INTRODUCTION

Quantum correlations (QCs) have become central for the characterization and the classification of quantum matters both in- and out-of-equilibrium [1–5]. Exotic quantum phases such as spin liquids [6, 7], topological [8–10], and many-body localized systems [11] have been manifested through QCs. It is demonstrated that entanglement in quantum many-body systems can be accessible in experiments such as in full-state tomography [12, 13] and ultra-cold atoms to measure Renyi entropies [14, 15] although these experimental efforts are limited to few-particle systems. Recently, using inelastic neutron scattering, an experimental protocol has been introduced to detect and quantify entanglement in the solid-state by performing measurements on Cs_2CoCl_4 , described as a quasi one-dimensional spin-1/2 XXZ model with a transverse field (TF) [16].

A growing interest in QCs – especially bipartite sites – has been intensified by the potential applications in information processing; for instance, continuous quantum machines [17], masking quantum information [18], quantum networks [19], and teleportation [20]. Due to the novelty of this topic, there are highly complicated problems to tackle to let us unravel the mystery of such systems. A crucial open proposal, here, is that to know how to set up a state (approximately) in equilibrium with a given Hamiltonian to gain more QCs than those in its ground state. In this paper, we strive hard to tackle this

problem in the framework of the nonequilibrium dynamics after a long-time evolution.

Non-equilibrium dynamic system compared to systems in equilibrium, is a far more complex topic. Therefore, quantum quenches provide a practical platform to examine the behavior of a system out of equilibrium [21–24]. The quenches can be global, local, or geometrical, i.e., an intermediate between a local and a global quench [25]. The essence of a quench outstandingly comes back to the different excess energy density measured with respect to the ground state energy of the post quench Hamiltonian. To clarify, in the global quenches, it remains finite while in the local quenches, when the system size increases, it vanishes. Recently, dynamical phase transitions in many body systems initially prepared in the state far-from-equilibrium have aroused considerable interest.

In the notation of the quantum quench, the concept of a *steady-state* transition describes a nonequilibrium quantum phase transition. In a sense, this transition is triggered by a nonanalytic change in physical properties as a function of the quench parameter in the asymptotic long-time average of the system [27]. Remarkably, the steady-state QCs shows a significant increase (a super-Heisenberg scaling) in comparison with those in the ground state [28]. This can be also applied to the dynamical quantum phase transition to characterize nonequilibrium criticality through the relationship of the singularities of Loschmidt echo to the zeros of local order parameters [29], the rate function and the fidelity susceptibility [30], the energy gap [31], and the delineation of the dynamical phase diagram of spin chains with long-range interactions [32].

In this paper, we are interested to know in what ways quench dynamics are more likely to affect steady-state

*Electronic address: smahdavifar@gmail.com

†Electronic address: h.cheraghi1986@gmail.com

QCs [33]. By employing concurrence and quantum discord (QD) as measures QCs in the system, we extract the features of the steady-state QCs after sudden quantum quenches at zero-temperature. The most striking fact that has been shown here is that this will lead to control and increase of QCs in the thermodynamic limit in the quantum spin-1/2 chains. This is more likely to allow us to identify quantum materials suitable for new applications and give us novel insights into complex quantum phenomena. Here, we focus on the integrable spin-1/2 XY chain model in a TF. It should be noted that our results can be applied to the other integrable and non-integrable models. The equilibrium phase diagram of the model at zero temperature is comprised of two phases, gapped ferromagnetic (FM) and paramagnetic (PM) phases separated at the critical field where a quantum phase transition occurs. We indicate that the quenching system from FM into PM regions creates a significant amount of QCs between nearest-neighbor pair spins in the long-time average. Moreover, a system exposed to the double quench provides the steady-state QCs at the final quenched point compared to both in equilibrium at $t = 0$ and in the steady-state of a single quench. In our setups, we make an effort to show the amplification of the steady-state QCs of system at the final quenched point λ_f (λ is control parameter) in phase C when it is initially placed at its ground state at λ_i in phase A . Here, to provide a double quench before the system to be quenched to λ_f , we seek an appropriate middle quenched point λ_m in phase B and a spending time T on which the system remains to control the values of the steady-state QCs at the final quenched point. Phases A , B , and C can be the same or not. We reasonably infer that by a proper protocol, a double quench can create more steady-state QCs than those in the single quench. More importantly, we find that the steady-state QCs – for both single and double quenches – disclose a singularity of the nonequilibrium quantum phase transition exactly at the quantum critical point, provided that the QCs do not undergo a sudden death in the vicinity of the critical point.

II. THE MODEL

We consider the Hamiltonian of the one-dimensional (1D) spin-1/2 XY model in the presence of a TF as

$$\mathcal{H} = -J \sum_{n=1}^N [(1 + \delta) S_n^x S_{n+1}^x + (1 - \delta) S_n^y S_{n+1}^y] - h \sum_{n=1}^N S_n^z, \quad (1)$$

where S_n is the spin operator on the n -th site. $J > 0$ denotes the FM exchange coupling. δ and h are the anisotropy parameter and the homogeneous TF, respectively. N is the system size (or number of spins) and

we consider the periodic boundary condition $S_{N+1}^\mu = S_1^\mu$ ($\mu = x, y, z$). The model exhibits a quantum phase transition at $h_c = J$ from the FM phase ($h < J$) to the PM phase ($h > J$) [34]. It can be seen that on the circle $h^2 + (J\delta)^2 = J^2$, the wave function of the ground state is factorized into a product of single spin states [35] that makes different regimes in the phase diagram of the model in the view of the revivals for Loschmidt echo [36].

The Hamiltonian is integrable and it can be mapped to a system of free fermions. This model is exactly solvable. By applying the Jordan-Wigner transformation [37], spins are mapped onto the one-dimensional noninteracting spinless fermions with the creation and annihilation operator,

$$\mathcal{H} = -\frac{J}{2} \sum_{n=1}^N [a_n^\dagger a_{n+1} + \delta a_n^\dagger a_{n+1}^\dagger + h.c.] - h \sum_{n=1}^N (a_n^\dagger a_n - 1/2), \quad (2)$$

where a_n is the fermionic operator. Performing a Fourier transformation as $a_n = (1/\sqrt{N}) \sum_k e^{-ikn} a_k$ makes the Hamiltonian as $\mathcal{H} = \sum_{k>0} H_k$ where $H_k = \mathcal{A}_k (a_k^\dagger a_k + a_{-k}^\dagger a_{-k}) + i\mathcal{B}_k (a_k^\dagger a_{-k}^\dagger + a_k a_{-k})$. A four-dimensional Hilbert space is spanned by the basis vectors $|0\rangle, |k\rangle = a_k^\dagger |0\rangle, |-k\rangle = a_{-k}^\dagger |0\rangle$, and $|k, -k\rangle = a_k^\dagger a_{-k}^\dagger |0\rangle$ where $|0\rangle$ is the vacuum state. Only bilinear terms like $a_k^\dagger a_{-k}^\dagger$ ensures that the parity of the total number of fermions provided by $n_k = a_k^\dagger a_k + a_{-k}^\dagger a_{-k}$ is conserved for each value of $k > 0$. Thus, the states $|0\rangle$ and $|k, -k\rangle$ are coupled to each other by the Hamiltonian, while the states $|k\rangle$ and $|-k\rangle$ remain invariant. Hence, in order to study the dynamics of the system, it is sufficient to project the Hamiltonian to the two dimensional subspace spanned by $|0\rangle$ and $|k, -k\rangle$ since the ground state for each value of k lies within this subspace. Using a Bogoliobov transformation presented by $a_k = \cos(\theta_k) \alpha_k + i \sin(\theta_k) \alpha_{-k}^\dagger$ leads to the quasiparticle diagonalized Hamiltonian as

$$\mathcal{H} = \sum_k \varepsilon_k (\alpha_k^\dagger \alpha_k - 1/2), \quad (3)$$

where the energy spectrum is $\varepsilon_k = \sqrt{\mathcal{A}_k^2 + \mathcal{B}_k^2}$ with

$$\mathcal{A}_k = -[J \cos(k) + h] \quad ; \quad \mathcal{B}_k = J\delta \sin(k), \quad (4)$$

and $\tan(2\theta_k) = -\mathcal{B}_k/\mathcal{A}_k$. For simplicity, we put $J = 1.0$. Thus, the quantum critical line is $h_c = 1.0$.

III. SETUPS AND TOOLS

Quantum many-body systems have been established to be a possible candidate for the implementation of quantum information protocols and powerful quantum computers [1–3]. with tools such as the entanglement and

the QD that are realized experimentally in various setups [38–40].

Also, numerous studies have been extended within the scope of the non-equilibrium dynamics of QCs in many-body system. [41–51]. Take the entanglement entropy, the entanglement spectrum [41, 42], and the quantum mutual information [43] as examples. It should be noted that there is a connection between the Schmidt gap and order parameters [44]. Moreover, the ratios of gaps of entanglement spectrum for a block of consecutive sites in the finite transverse field Ising chains are geared to obtaining universal information [45]. In systems weakly coupled to a dephasing Markovian environment, entanglement and quantum mutual information play a crucial role in destroying many-body localization [46] and propagating QCs [47]. Entanglement spectrum causes emergence of the dynamical quantum phase transition [48]. The entanglement entropy is exerted to examine the propagation of non-local QCs in a quench from the hermitian to the non-hermitian models [49]. The most telling point in the study of the dynamics of the pairwise entanglement and the quantum discord (QD) in the spin-1/2 XXZ chain model [50] is that contrary to the concurrence, QD emerges as a good identifier of a quench by revealing some nonanalytic behaviors when it exceeds critical points. Further, multipartite entanglement turns out to be useful for the mentioned detection [51].

Having been confirmed the importance of the existence of QCs in executing quantum tasks, it is vital to seek quantum systems with enough QCs especially at zero-temperature and approximately in equilibrium with a state under given circumstances in which the system reaches a steady-state. To this end, with the use of the quench dynamics, we suggest a setup that provides more QCs in spin-1/2 quantum chains. The most noticeable fact is that the larger quench gap necessarily does not produce the larger steady-state QCs. It crucially depends on how the setup launches. Accordingly, our results presented here are different from what has been reported for the entanglement entropy [52]. In this work, by employing a single and a double quench together with the conception of steady-state, we change the nature of the system so that the particles of the many-body quantum system are forced to feel more QCs at the long-time average of the system. Due to the rich structure of many-body states, a number of different QCs measures have been introduced. Here, we examine the QCs in a bipartite system with QD and concurrence measures at zero-temperature. These measures quantify all correlations between two sites that reveal information about the system [1–3, 17–20].

A. Setups

We first fix the initial state of the system into the ground state of the initial Hamiltonian $\mathcal{H}(\lambda_i)$, where λ indicates a control parameter that can be one or more.

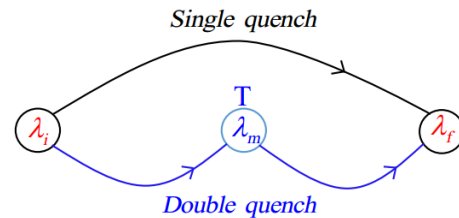


FIG. 1: The schematic diagram of the setups.

Then, we use the idea of single quench and double quench for the system as the following:

(i) For single quench, at $t = 0$, a quench starts from an initial state (in phase A) to a final state (in phase C), as λ_i to λ_f .

(ii) For double quench, at $t = 0$, a quench starts from an initial state (in phase A) to a middle state (in phase B), as λ_i to λ_m , and then a quench at $t = T$ from an evolved state (in phase B) to a final state (in phase C), as λ_m to λ_f . Phases A , B , and C may be the same or not.

The time-dependent Hamiltonian $\mathcal{H}(t)$ that models a double quantum quench is

$$\mathcal{H}(t) = \begin{cases} \mathcal{H}(\lambda_i), & t \leq 0 \\ \mathcal{H}(\lambda_m), & 0 \leq t \leq T \\ \mathcal{H}(\lambda_f), & t \geq T \end{cases} \quad (5)$$

with $|\Psi(\lambda_i)\rangle$ and $|\Psi(\lambda_m)(T)\rangle = e^{-iT\mathcal{H}(\lambda_m)}|\Psi(\lambda_i)\rangle$ that are the initial state at $t = 0$ and the evolved state at $t = T$, respectively. The setups are schematically represented in Fig. 1. Accordingly, the system needs to be investigated in a long-time average at the final quenched point λ_f where it fluctuates slowly around a stable situation at a steady-state. A system is in a steady-state if the expectation values of local observable quantities become almost time-independent, by taking the limit $t \rightarrow \infty$ [27–32]. The nature of such a steady-state has been discussed in terms of the eigenstate thermalization hypothesis (ETH) [53–56] that is beyond the main theme of this work. The main purpose of this paper is to indicate that this protocol helps us control and boost the values of the QCs at the long-time average of the system instead of QCs in the zero-temperature value at the final quenched point λ_f . The control of amplifying steady-state QCs in the system will be attainable in phase B by adjusting the middle quench point λ_m and the spending time T , defined as the time passing from the middle quench point before the system is exposed to a second quench.

B. Tools

. *Concurrence.*— The concurrence is a measure of entanglement between two spins at sites i and j (here, we

consider nearest-neighbors, $j = i + 1$). It can be obtained from the corresponding reduced density matrix $\rho_{i,i+1}$ [57]. In the fermionic picture, the reduced density matrix for two-point correlation functions can be written as

$$\rho_{i,i+1} = \begin{pmatrix} X_{i,i+1}^+ & 0 & 0 & -f_{i,i+1}^* \\ 0 & Y_{i,i+1}^+ & Z_{i,i+1}^* & 0 \\ 0 & Z_{i,i+1}^- & Y_{i,i+1}^- & 0 \\ f_{i,i+1} & 0 & 0 & X_{i,i+1}^- \end{pmatrix}, \quad (6)$$

where

$$\begin{aligned} X_{i,i+1}^+ &= \langle n_i n_{i+1} \rangle, \\ Y_{i,i+1}^+ &= \langle n_i (1 - n_{i+1}) \rangle, \\ Y_{i,i+1}^- &= \langle n_{i+1} (1 - n_i) \rangle, \\ Z_{i,i+1} &= \langle a_i^\dagger a_{i+1} \rangle, \\ X_{i,i+1}^- &= \langle 1 - n_i - n_{i+1} + n_i n_{i+1} \rangle, \\ f_{i,i+1} &= \langle a_i^\dagger a_{i+1}^\dagger \rangle, \end{aligned} \quad (7)$$

that $n_i = a_i^\dagger a_i$ is a fermionic occupation number of the i -th mode. Therefore, the concurrence of the density matrix is given by

$$C(\rho_{i,i+1}) = \text{Max}[0, \Lambda_1, \Lambda_2], \quad (8)$$

with

$$\begin{aligned} \Lambda_1 &= 2(|Z_{i,i+1}| - (X_{i,i+1}^+ X_{i,i+1}^-)^{1/2}), \\ \Lambda_2 &= 2(|f_{i,i+1}| - (Y_{i,i+1}^+ Y_{i,i+1}^-)^{1/2}). \end{aligned} \quad (9)$$

Quantum discord.— To capture all QCs in a bipartite state that are not revealed by the concurrence [58, 59], one calculates the QD [60]. The QD is defined by the difference between total correlation, $\mathcal{I}(\rho_{i,i+1})$, and classical correlation, $\mathcal{C}(\rho_{i,i+1})$, as

$$QD_{i,i+1} = \mathcal{I}(\rho_{i,i+1}) - \mathcal{C}(\rho_{i,i+1}). \quad (10)$$

To calculate the total and classical correlations, we use the reduced density matrix (eq. (7)) [61]. In Appendix A, the derivation of the QD is explained in detail.

In the nonequilibrium dynamics of the system, the time-dependent two-point correlation functions are essential to derive the two sites reduced density matrix, given as

$$R(t) = \frac{1}{N} \sum_{l=1}^N \langle a_l^\dagger a_{l+1} \rangle ; \quad S(t) = \frac{1}{N} \sum_{l=1}^N \langle a_l^\dagger a_{l+1}^\dagger \rangle$$

which for the first quench, it is given by

$$\begin{aligned} R(t) &= \frac{1}{N} \sum_{k>0} \cos(k) \left[1 - \cos(2\theta_k^f) \cos(2\Phi_k^f) \right. \\ &\quad \left. - \sin(2\theta_k^f) \sin(2\Phi_k^f) \cos(2\varepsilon_k^f t) \right], \\ S(t) &= \frac{1}{N} \sum_{k>0} \sin(k) \sin(2\Phi_k^f) \left[\frac{\sin(2\theta_k^f)}{\tan(2\Phi_k^f)} \right. \\ &\quad \left. - \cos(2\theta_k^f) \cos(2\varepsilon_k^f t) - i \sin(2\varepsilon_k^f t) \right], \end{aligned} \quad (11)$$

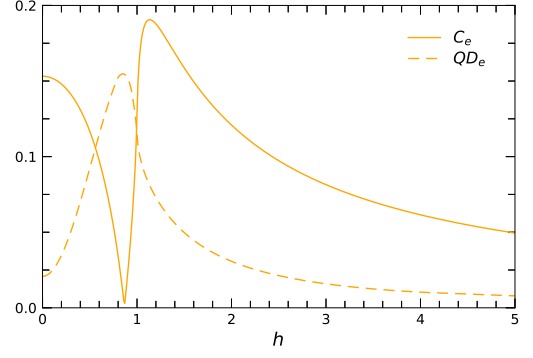


FIG. 2: The equilibrium values of the concurrence (solid plot) and the QD (dashed plot) at $t = 0$ for the nearest-neighbor pair spins as a function of the TF for $\delta = 0.5$.

with $\Phi_k^f = \theta_k^f - \theta_k^i$.

Also, for the second quench for $t \geq T$, it is as following

$$\begin{aligned} R(t) &= \frac{2}{N} \sum_{k>0} \cos(k) |Q_k(t)|^2, \\ S(t) &= -\frac{2}{N} \sum_{k>0} \sin(k) Q_k^*(t) P_k^*(t), \end{aligned} \quad (12)$$

where

$$\begin{aligned} P_k(t) &= p_k(t) \cos(\Phi_k^m) e^{-iT\varepsilon_k^m} \\ &\quad + q_k(t) \sin(\Phi_k^m) e^{iT\varepsilon_k^m}, \\ Q_k(t) &= q_k(t) \cos(\Phi_k^m) e^{iT\varepsilon_k^m} \\ &\quad - p_k(t) \sin(\Phi_k^m) e^{-iT\varepsilon_k^m}, \end{aligned}$$

with

$$\begin{aligned} p_k(t) &= \cos(\theta_k^f) \cos(\Phi_k^f) e^{-i(t-T)\varepsilon_k^f} \\ &\quad + \sin(\theta_k^f) \sin(\Phi_k^f) e^{i(t-T)\varepsilon_k^f}, \\ q_k(t) &= \sin(\theta_k^f) \cos(\Phi_k^f) e^{i(t-T)\varepsilon_k^f} \\ &\quad - \cos(\theta_k^f) \sin(\Phi_k^f) e^{-i(t-T)\varepsilon_k^f}, \end{aligned}$$

that we have used $Q_{-k}(t) = -Q_k(t)$ and $P_{-k}(t) = P_k(t)$. For the second quench, the quantity $\Phi_k^{f/m} = \theta_k^{f/m} - \theta_k^{m/i}$ is the difference between the Bogoliubov angles diagonalizing the pre-quench and the post-quench Hamiltonians. θ_k^i belongs to the energy spectrum ε_k^i with similar definitions for θ_k^m and θ_k^f .

IV. RESULTS AND DISCUSSIONS

We first should mention that before a quench in which the system is in an equilibrium situation, the QCs between nearest-neighbor pair spins in the ground state are known. The graph in Fig. 2 provides information about the equilibrium values of the concurrence (C_e) and

the QD (QD_e) for the nearest-neighbor pair spins versus the TF for $\delta = 0.5$. It is noticeable that at the factorized point, the concurrence is zero while the QD reaches its maximum value [62]. With the increase of the TF, the concurrence first grows swiftly, and peaks around the critical TF, and then falls exponentially. This pattern is the same for QD. In the following, we argue about the steady-state QCs for the nearest-neighbor pair spins in the quench dynamics of the system. In this spirit, the long-time average of a parameter \mathcal{O} , (as $\langle \mathcal{O} \rangle = \lim_{\tau \rightarrow \infty} \frac{1}{\tau} \int_0^\tau \mathcal{O}(t) dt$) lead to the system lies in the steady-state. In the subsequent numerical plots without losing generality, we put a fixed anisotropy parameter as $\delta = 0.5$.

A. Single quench

In a single quench, a system first is initially prepared in its ground state at h_i , where h_i is the transverse field, then the TF is switched suddenly to a final value h_f . Now, using the time evolution operator, we seek the dynamic of the system. In Fig. 3, we have shown the steady-state concurrence and the steady-state QD versus the final TF. Figures. 3(a) and 3(c) correspond in the quenches in the FM phase. As it can be seen, for quenches in the PM phase, at the long-time, both the concurrence and the QD will share greater steady-state QCs between nearest-neighbor pair spins compared to QCs in equilibrium states. The reason behind this is that, in the PM phase, the system in the equilibrium is almost polarized while the time-dependent physical state is a superposition of the ground and the excited states of the Hamiltonian at the final quenched point. Figures. 3(b) and 3(d) indicates the steady-state QCs versus final TF where quenches are in the PM phase. As a consequence, this process is unable to produce the QCs more than the system in the equilibrium.

It should be mentioned that all quenches applied to the quantum critical point, $h_f = 1.0$, lead to a steady-state QC with a nonanalyticity, displaying a nonequilibrium phase transition with h_f as a control parameter. This is similar to the results for the model in which long-time average of the order parameters disclose nonequilibrium quantum criticality when quenching crosses an equilibrium quantum critical point [29–32, 63]. However, in this present study, a nonanalyticity appears only when the final quenched point itself is in a critical point. Since the properties of the proposed nonequilibrium criticality in Fig. 3 are of interest, in Appendix B, we address it by making a comparison between the steady-state QCs and Loschmidt echo.

Now, we speculate the role of the excited states emerged from the dynamics of the system to create or annihilate the entanglement in long-time dynamics of the system. The time-dependent physical state of the system can be written as $|\Psi(t)\rangle = \sum_{n=0} g_n e^{-iE_n^f t} |E_n^f\rangle$, where the eigenvalues $\{E_n^f\}$ and eigenvectors $\{|E_n^f\rangle\}$ with

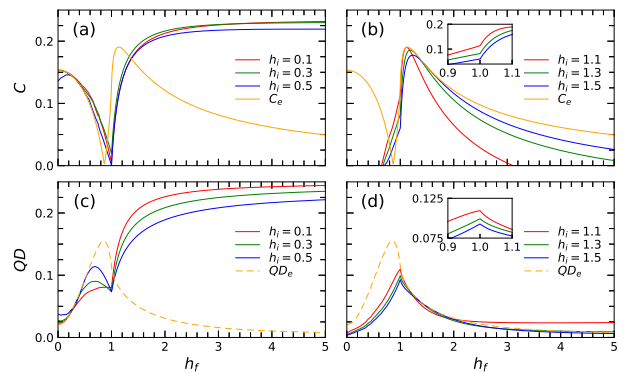


FIG. 3: (color online) The steady-state QCs as a function of final TFs for quenches from (a), (c) the FM phase, and (b), (d) the PM phase. For more clarity of non-analytic behaviors of Figs. (b) and (d) at the quantum critical point $h_c = 1.0$, we have added their insets.

$n = 0, 1, 2, \dots$, corresponding to the Hamiltonian at the quenched point. In addition, the expansion coefficients are $g_n = \langle E_n^f | \Psi(0) \rangle$. The exact solution for the expansion coefficients is as

$$g_n = \prod_{k>0} \langle E_n^f | [\cos(\Phi_k^f) - i \sin(\Phi_k^f) \alpha_k^{\dagger f} \alpha_{-k}^{\dagger f}] | E_0^f \rangle. \quad (13)$$

where α_k^f is related to the quasi-particle diagonalizing the quenched Hamiltonian. The time-dependent concurrence can be written as

$$C(t) = \sum_n |g_n|^2 C_n + \sum_{n \neq n'} g_n^* g_{n'} e^{-i(E_{n'}^f - E_n^f)t} C_{n,n'} \quad (14)$$

with $C_{n,n'} = \langle E_n^f | C | E_{n'}^f \rangle$. At long-time average, the steady-state concurrence yields to

$$\langle C \rangle = |g_0|^2 C_0 + \sum_{n \neq 0} |g_n|^2 C_n, \quad (15)$$

where C_n indicates the value of concurrence in the excited states of the quenched Hamiltonian. For the ground state, we have $n = 0$ and $g_0 = \prod_{k>0} \cos(\Phi_k^f)$. As can be seen from eq. (14), the time-dependent concurrence is composed of two terms, one of which is constant and the other is time-dependent. By applying the long-time average condition, we extract eq. (15) that reveals the steady-state concurrence. It can be inferred that only this term plays a significant role in the steady-state concurrence.

A notable feature in eq. (13) is that only subspaces with an even-number of fermions should be explored. In other words, g_n for an odd-number of fermions is zero. In Fig. 4(a), $|g_0|$ is plotted versus quenched TF for initial states in the FM, PM phase, and the critical point. It is clear that $|g_0| = 1$, only happens when there is no

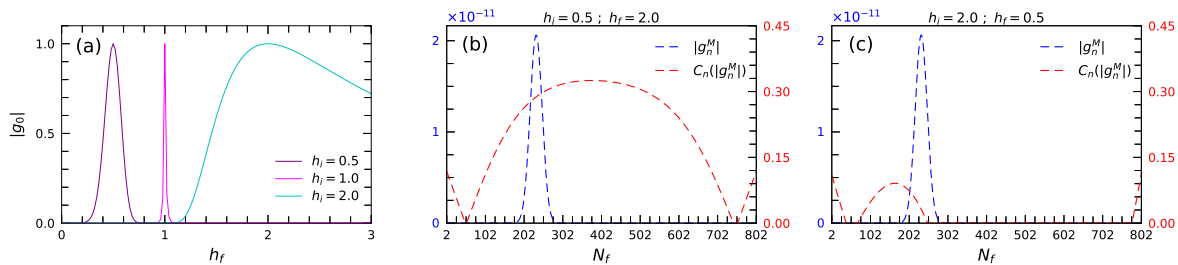


FIG. 4: (color online) (a) The expansion coefficient $|g_0|$ versus h_f for quenches from $h_i = 0.5, 1.0, 2.0$. The maximum values of the expansion coefficients (for $n \neq 0$) and associated entanglements are demonstrated versus the occupation number N_f for quenches from (b) $h_i = 0.5$ to $h_f = 2.0$, and (c) $h_i = 2.0$ to $h_f = 0.5$. Here, the system size is $N = 800$.

quench. Another point to be noted is that since quenching from one phase into another breaks the symmetry of the ground state, $|g_0|$ tends to be zero. As a result, high excited states can contribute significantly to the steady-state concurrence. To seek more information about the role of the excited states, we have calculated the maximum values of the expansion coefficient $|g_n^M|$ in the different even-subspaces in the interval $k \in [0, \pi]$. By doing so, we detect a special wave number k^* . The results are illustrated for a quench from the FM to the PM phases in (Fig. 4(b)) and then from the PM to the FM phases in (Fig. 4(c)) for a chain with size $N = 800$ as a function of the occupation number N_f , as $N_f = \sum_k \langle E_n^f | \alpha_k^\dagger \alpha_k^f | E_n^f \rangle$. It should be mentioned that $|g_n^M|$ is the same for both cases. Regions with a high number of fermions, it reached to the highest value in which the energy spectrum contains high energy excited branches. Moreover, the concurrence belonging to $|g_n^M|$ reveals different behaviors. As shown, its amount in the overlapping region, for panel (b) is more than panel (c). The most noticeable point is that in the high energy excited branches, the pair spins for quenches from the FM to the PM phases are entangled in all subspaces and they display a complete overlapping with $|g_n^M|$. That is why we witness a significant value of the entanglement ($\sum_{n \neq 0} |g_n|^2 C_n$) that is considerably larger than its ground state value. In contrast, in a quench from the PM to the FM phases, the overlap is restricted to a part (panel(c)). Consequently, that similar to the former, where quench does not happen.

A deeper insight into the quench dynamics of the system is investigated by focusing the role of the initial state on the amount of the steady-state QCs at the final quenched point. The graphs, in Fig. 5, compare figures for different values of h , specifically at $h_f = 0.5, 5.0$. It is illustrated that when quenches is applies to the PM phase, with initial state in the FM phase, it leads to more QCs compared to the case in which the initial state is in the PM phase. Moreover, the QCs for the initial states in the PM phase far from the quantum critical point reveal a constant value close to the equilibrium, independent of the initial state though. For the QD, this value is almost zero. Another point to be mentioned is that in the PM phase, there is a region very close to $h_c = 1$ where the

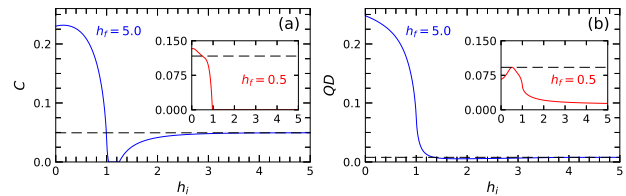


FIG. 5: (color online) The steady-state (a) concurrence and (b) QD as a function of initial TFs for quenches into the PM phase (the plots) and the FM phase (the insets), respectively. The horizontal black dashed lines indicates the QCs in the equilibrium at h_f .

concurrence is zero. The pattern is reverse for the QD in which it is more than its equilibrium. However, the insets of Fig. 5 are related to quenches from the desired initial states into a final quenched point in the FM phase as $h_f = 0.5$. Based on the exact results, for an initial state within the PM phase, the pair spins will not entangle at long times. To put it more simply, the concurrence does not exist while the QD is minor. Also, only initial states within $h_i < h_f$ can have more entanglement values than their equilibriums. It should be noted that the initial states always generate the steady-state QD less than its equilibrium.

B. Double quench

To study the dynamics of the QCs in the double quench dynamics, we apply a middle quenched point h_m before the system is exposed to a quench from the initial point h_i to the final point h_f . In the middle quenched point, the system will evolve up to the given time $t = T$. At this specific time, the system is exposed to the second quench and it continues to evolve into the final Hamiltonian. Both control parameters, h_m and T are responsible for controlling the value of the steady-state QCs in the final quenched point.

In Fig. 6, we plot the steady-state concurrence and the QD versus the spending time T for the different middle

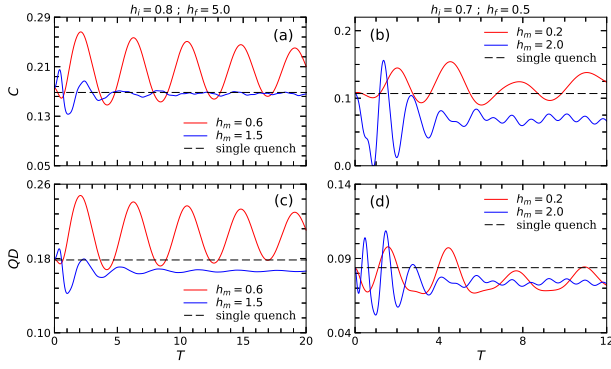


FIG. 6: (color online) The steady-state QCs versus the spending time T for a quench from (a), (c) $h_i = 0.8$ to $h_f = 5.0$ and (b), (d) $h_i = 0.7$ to $h_f = 0.5$, where middle quenched points are situated at the FM and the PM phases. The horizontal black dashed lines illustrates the steady-state QCs for the single quench case as $h_i \rightarrow h_f$.

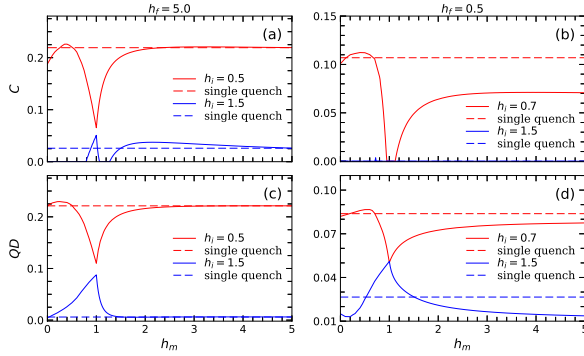


FIG. 7: (color online) The steady-state QCs as a function of h_m when the system is in a steady-state at the middle point for quenches from the FM and the PM phases into final points $h_f = 0.5, 5.0$. The horizontal black dashed lines illustrates the steady-state QCs for the single quench case as $h_i \rightarrow h_f$.

points h_m . Also, the steady-state QCs for a single quench from h_i to h_f are shown by the horizontal black dashed lines.

The main purpose of this work is to explore amplified values of the QCs at a final quenched point into both the FM and the PM phases as $h_f = 0.5; 5.0$. Here, the system initially is placed in the FM phase. We elect two middle points; one in the FM phase, and another in the PM phase. As it is evident, by selecting out an appropriate middle point in the FM and the PM phase, some given spending times will appear at which the system can gain more QCs. The most intriguing fact is that, in some specific times, the QCs for the second quench are exactly the same as QCs in the single quench. This is common to protocols in which the QCs in double quench cross QCs in single quenches. It shows that neither h_m nor spending time T has an impact on steady-state QCs.

A notable feature in Fig. 6 is that for the middle point, in the FM phase, the oscillations spread on larger spend-

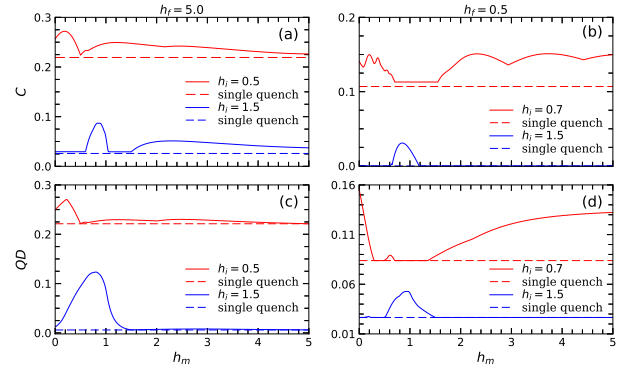


FIG. 8: (color online) The same as Fig. 7 with the difference that here at the middle point, the time T is chosen from the interval $[0,10]$ in such a way that it belongs to the maximum value of QCs.

ing time T that is vividly illustrated in panels (red color). The steady-state QCs oscillate around a mean value – faster or slower depending on the type of quench – and with a quench-dependent period T_{osc} . For the middle point in the PM phase, the pattern is the same while a small irregularity arises. Moreover, it can be inferred from Fig. 6(a), (c) and Fig. 6(b), (d) that T_{osc} for a certain quench (e.g. $h_i=0.8, h_f=0.5$), the QCs in the PM phase coincide with those in the FM phase. By Intuition, for the middle point in the PM phase, the steady-state QCs at the middle point damp sharply at the short spending timing spend T ((time measure shown in the Fig) (blue color). For these chosen quenches, panels (a)-(c) reveal that if the system stays in the middle point in the FM phase for a long-time, we can capture more steady-state QCs than those in the single quench. In contrast, this case never arises from the middle point in the PM phase.

Eventually, we investigate how the middle point affects the steady-state QCs in the process of the double quench dynamics. First, we explore the behavior of QCs when the system reaches a steady-state situation in the middle point (Fig. 7). Fig. 7 shows changes in the steady-state QCs as a function of h_m when the system is in a steady-state at the middle point for quenches originated from the FM and the PM phases into final points $h_f = 0.5; 5.0$.

Then, we examine the behavior of QCs, when the system is exposed to the double quench at a specific time where the QCs have their maximum values. (Fig. 8). In the latter case, we let the system evolves at the middle point up to $T = 10$ and we elect the maximum of the QCs in this interval. So the spending time for the latter varies. The results demonstrated in Figs. 7 and 8 correspond to quenches from different initial and final states of the FM and the PM phases into desired middle points. As shown in Fig. 7, a steady-state situation in the middle point is unable to create remarkable values of the QCs, while we witness amplified QD at h_i in the PM phase. The

quantum critical point at h_m in the steady-state situation unveil an explicit signature by generating minimum and maximum values and a nonanalytic behavior of a nonequilibrium phase transition exactly at the equilibrium critical point, provided that sudden death does not occur (please see Appendix B). The quenching at a given time T when the QCs achieve the maximum value at an optional interval $T = [0, 10]$, makes the possibility of attaining more steady-state QCs in double quenches than those in single quenches (Fig. 8). As a consequence, to have QCs more than both the ground-state and the single quench is possible by properly adjusting the middle point and timing spend T . To harness more QCs than those in the ground-state and the single quench seems technically feasible in the double quench through adjusting the middle point and spending time T .

V. CONCLUSION

Quantum information relies on operations beyond classical ones that nowadays experimentally is feasible by ultracold atoms and molecules in optical lattices as the nearly ideal platform for studying quantum many-body systems [12–14]. To perform quantum tasks, the system under study must have a sufficient QC. To gain the dramatic amount of QCs in a quantum system that is not necessarily in its ground state is one of the challenges at the study of quantum processes.

We proposed a way in which a state is almost in equilibrium with the system to provide more QCs. This protocol facilitates the study of quantum procedures even in the systems with small QCs in their ground states. This study is based on quantum quench, i.e., a simple protocol to bring a system out of equilibrium. In fact, the goal is to generate the steady-state QCs by the quench dynamics in the long-time evolution. Due to the exact solvability of several 1D quantum systems that represent an ideal framework corresponding to experimental data, in this paper, we focused on the 1D spin-1/2 XY model in the presence of a TF. The motivation behind this paper is that the integrable 1D many-body models can be experimentally engineered and their nonequilibrium dynamics have been investigated in more detail in many contexts [26, 33].

We here established our setups upon single and double quantum quenches subjected by a TF, and investigated the steady-state QCs in the final quenched points. It has been shown that how one can gain a more steady-state QCs than those in the ground state while we use concurrence and QD as measures of QCs. A single quench from the FM into the PM phases showed up an outstanding amount of QCs while the same pattern is not seen from the PM to FM phases. To address this issue, we put forward an analytical relationship for the steady-state concurrence and inferred that for the former case, there is an entirely overlap between the maximum values of the expansion coefficients and related concurrence while for

the latter one, it is not seen.

In the next step, we wonder if it is possible to increase the QCs more? To explore it, we used an interesting idea, a double quench, as a way that the system before locating in the final point will be quenched to a middle point and we evaluated the system at this point for a given time T . Afterwards, at the time T , the system is exposed to the second quench. Spending time T can be for a short time or for a long-time so that the system sets in a steady-state situation at the middle point. Furthermore, the middle point can be chosen in the FM or the PM phases. The aim is to select the middle point and spending time so that the system achieves a greater steady-state QCs at the final point compared to the single quench. Our results clearly demonstrated that this can be feasible through the control of these parameters.

Additionally, it has been shown that nonequilibrium quantum phase transitions can be identified by non-analyticities in the long-time average of some parameters such as order parameters, Loschmidt echo, and quantum Fisher information when the quenched parameter as the control parameter crosses the critical point. Here, we extended this topic to the QCs and proved that a nonanalyticity will emerge if the final magnetic field as a control parameter crosses the critical point when the system is placed at a steady-state with the condition that the sudden death does not occur at or around the critical point. In Appendix B, we tackle this matter in detail.

It can be inferred that all these results have been established based on a basic theoretical framework, simply applied to other complex models. Moreover, it can be predicted that such a framework is more likely to be upgraded to higher quenches (triple,...) to create more QCs compared to double quenches.

Acknowledgment.— H. Cheraghi thanks National Science Centre (NCN, Poland) under Grant No. 2019/35/B/ST3/03625. for the support of this work. We are also thankful to T. Mohammad Alizadeh and J. Vahedi for proofreading and editing the article.

Appendix A: Quantum discord

The total correlation can be calculated by

$$\mathcal{I}(\rho_{i,i+1}) = S(\rho_i) + S(\rho_{i,i+1}) + \sum_{\alpha=0}^3 \lambda_{\alpha} \log_2 \lambda_{\alpha}, \quad (\text{A1})$$

where λ_{α} is the eigenvalue of the density matrix $\rho_{i,i+1}$, and

$$S(\rho_i) = - \sum_{\xi=\pm 1} \left[\frac{1 + \xi c_4}{2} \log_2 \left(\frac{1 + \xi c_4}{2} \right) \right]. \quad (\text{A2})$$

Here, $c_{i=1,\dots,4}$, are expressed as

$$\begin{aligned} c_{1/2} &= 2(Z_{i,i+1} \pm f_{i,i+1}), \\ c_{3/4} &= X_{i,i+1}^+ \pm X_{i,i+1}^- - Y_{i,i+1}^+ \mp Y_{i,i+1}^-. \end{aligned} \quad (\text{A3})$$

Since the translational invariance of the original Hamiltonian, the single-site density matrices ρ_i and $\rho_{i,i+1}$ are equal, we have $S(\rho_i) = S(\rho_{i,i+1})$.

The calculation of the classical correlation $\mathcal{C}(\rho_{i,i+1})$ requires an optimization over rank-1 local measurements on part B of $\rho_{i,i+1}$ (here we have taken site j of $\rho_{i,j}$ as part B). A general set of local rank-1 measurement operators, B_0, B_1 , can be defined as $B_{k'=0/1} = V \prod_{k'} V^\dagger$, where $V \in U(2)$ and the projectors $\prod_{k'}$ are given in the computational basis $|0\rangle \equiv |\uparrow\rangle$ and $|1\rangle \equiv |\downarrow\rangle$. The post measurement outcomes get updated to one of the following states

$$\rho_{k'} = \left(\frac{1}{2} + \sum_{j=1}^3 \chi_{k'} S_j \right) \otimes (V \prod_{k'} V^\dagger), \quad (\text{A4})$$

where the elements of the density matrices are given by

$$\begin{aligned} \chi_{k'i=1,2} &= \frac{(-1)^{k'} c_i \sin \theta \cos \phi}{1 + (-1)^{k'} c_4 \cos \theta}, \\ \chi_{k'3} &= \frac{(-1)^{k'} c_3 \cos \theta + c_4}{1 + (-1)^{k'} c_4 \cos \theta}. \end{aligned} \quad (\text{A5})$$

Here, the azimuthal angle $\theta = [0, \pi]$ and the polar angle $\phi = [0, 2\pi]$ represent a qubit over the Bloch sphere. By considering the normalization of the density matrices, $\theta_{k'} = (\sum_{j=1}^3 \chi_{k'j}^2)^{1/2}$, we derive the classical correlation between the spin pairs

$$\begin{aligned} \mathcal{C}(\rho_{i,i+1}) &= \text{Max}_{\{B_{k'}\}} \left[S(\rho_i) - \frac{S(\rho_0) + S(\rho_1)}{2} \right. \\ &\quad \left. - c_4 \cos \theta \frac{S(\rho_0) - S(\rho_1)}{2} \right], \end{aligned} \quad (\text{A6})$$

where the von Neumann entropies are given by

$$S(\rho_{k'}) = - \sum_{\xi=\pm 1} \left[\frac{1 + \xi \theta_{k'}}{2} \log_2 \left(\frac{1 + \xi \theta_{k'}}{2} \right) \right]. \quad (\text{A7})$$

It should be noted that the von Neumann entropy of $V \prod_{k'} V^\dagger$ is zero.

Appendix B: Nonanalyticity at the quantum critical point in the steady-state QCs

A quench from a noncritical point to a critical point at the long time average of the system leads to the emergence of nonanalytical behaviors of the steady-state QCs. It occurs when the quenched parameter as control parameter crosses the critical point, and the critical point will be far from the sudden death phenomenon. We here are going to extract the origination of these nonanalytics.

Single quench.— In general, we assume an initial Hamiltonian $\mathcal{H}(h_i)$ at $t = 0$ in the equilibrium with its ground state. It undergoes a quantum quench from h_i

to h_f that puts the system in a nonequilibrium condition. Loschmidt echo is defined as the overlap between initial and time-evolved states, $LE(t) = |\langle \Psi(0) | \Psi(t) \rangle|^2$. It is demonstrated that nonequilibrium quantum phase transitions can be identified by nonanalyticities in the long-time average of the Loschmidt echo, written as [30]

$$\bar{\mathcal{L}}(h_f) = \sum_n |\langle E_n^f | \Psi(0) \rangle|^4 = \sum_n |g_n|^4 \quad (\text{B1})$$

In fact, at the critical point the sharp of $\bar{\mathcal{L}}$ changes and thus the rate function, i.e., the logarithm function of Loschmidt echo, can exactly give the quantum critical point. With the comparison of eq. (B1) and eq. (15), it is easy to prove that the nonanalytical behaviors existing in $h_f = 1$ are hidden in the heart of the g_n parameter where h_f as the control parameter crosses the critical point.

Let us come back to the theory of the dynamical quantum phase transition [26] where the Fisher zeros of Loschmidt echo are $z_l = [\ln(\tan^2(\Phi_k^f)) + i\pi(2l+1)]/(2\varepsilon_k^f)$, with $l = 0, 1, 2, \dots$. As known, nonanalytic behaviors of the rate function in the form of cusps at some special times called *critical times* occurs in Fisher zeros. When $\Phi_k^f = \pm\pi/4$, the real parts of z_l are zero, and we get the critical times $t_l = t^*(l+1/2)$ with $t^* = \pi/\varepsilon_{k^*}^f$ where k^* is the particular mode driven from $\cos(2\Phi_{k^*}^f) = 0$. If the pre-quenched Hamiltonian is in noncritical point but the post-quenched Hamiltonian is in critical, there is no dynamical quantum phase transition in finite time [64]. In this case, $k^* = \pm\pi$ is also the gap-closing point of the post-quenched Hamiltonian, i.e., $\varepsilon_{k^*}^f = 0$. Instead, in this situation $t^* = \infty$. At the long time average of the system, the nonanalytic point as a cusp appears. Similarity, we should accept the nonanalytics of the steady-state QCs of the system after a long-time evolution. In addition, $k^* = \pm\pi$ leads to the singularity of the Bogoliubov angle at the gap-closing momentum [64]. In a sense, all g_n can play a role to create the nonanalyticity at the critical point.

Double quench.— A double quench is defined as a quench from h_i to h_m and then at T , from h_m to h_f . For the single quench $h_i \rightarrow h_m$ at $t = T$ we have

$$|\Psi(T)\rangle = e^{-iTH^m} |\Psi(0)\rangle = \sum_{p=0} g_p e^{-iT E_p^m} |E_p^m\rangle \quad (\text{B2})$$

where $g_p = \langle E_p^m | \Psi(0) \rangle$. Now, the second quench for $t > T$ is given by

$$\begin{aligned} |\Psi(t)\rangle &= e^{-i(t-T)H^f} |\Psi(T)\rangle \\ &= \sum_{p,q=0} g_p d_q e^{-iT(E_p^m - E_q^f)} e^{-itE_q^f} |E_q^f\rangle \end{aligned} \quad (\text{B3})$$

where $d_q = \langle E_q^f | E_p^m \rangle$. So, the long-time average of the Loschmidt echo and the concurrence are as the following

$$\bar{\mathcal{L}}(h_f) = \sum_{p,q,w=0} |g_p|^2 |g_w|^2 |d_q|^2 |d_w|^2$$

$$\langle C \rangle = \sum_{p,q=0} |g_p|^2 |d_q|^2 C_{q,q} \quad (\text{B4})$$

where $C_{q,q} = \langle E_q^f | C | E_q^f \rangle$. By comparing these equations one concludes that the nonanalyticity in Loschmidt echo directly is related to g_p, g_w, d_q and d_w which are parameters that construct the concurrence. For this case, the critical times arisen from zeros of Loschmidt echo are $t_l^* = \frac{\pi}{2\varepsilon_{k^*}^f} [(2l+1) - \varphi_{k^*}]$, with $l = 0, 1, 2, \dots$, where φ_{k^*}

is a phase shift originated from the time evolution for $t < T$ [65]. Here, for $h_f = 1.0$ we infer that $k^* = \pm\pi$ is the gap-closing point of the post-quenched Hamiltonian, and hence $\varepsilon_{k^*=\pm\pi}^f = 0$. Therefore, we extract the same results as what we have for the single quench, unveiling the nonanalyticity at the steady-state QCs.

-
- [1] A. Osterloh, L. Amico, G. Falci, R. Fazio, *Nature* **416**, 608, (2002); L. Amico, R. Fazio, A. Osterloh and V. Vedral, *Rev. Mod. Phys.* **80**, 517 (2008).
- [2] R. Horodecki, P. Horodecki, M. Horodecki and K. Horodecki, *Rev. Mod. Phys.* **81**, 865 (2009).
- [3] A. Bera, T. Das, D. Sadhukhan, S. S. Roy, A. Sen and U. Sen, *Rep. Prog. Phys.* **81**, 024001 (2018).
- [4] D. Braun, G. Adesso, F. Benatti, R. Floreanini, U. Marzolino, M. W. Mitchell, S. Pirandola, *Rev. Mod. Phys.* **90**, 35006 (2018).
- [5] J. T. Schneider, J. Despres, S. J. Thomson, L. Tagliacozzo, and L. Sanchez-Palencia, *Phys. Rev. Research* **3**, L012022 (2021).
- [6] L. Balents, *Nature* **464**, 199 (2010).
- [7] L. Savary and L. Balents, *Rep. Prog. Phys.* **80**, 016502 (2017).
- [8] F. Pollmann, A. M Turner, E. Berg, and M. Oshikawa, *Phys. Rev. B* **81**, 064439 (2010).
- [9] H.-C. Jiang, Z. Wang, and L. Balents, *Nat. Phys.* **8**, 902 (2012).
- [10] T. Haug, L. Amico, L.-C. Kwek, W. J. Munro, and V. M. Bastidas, *Phys. Rev. Research* **2**, 013135 (2020).
- [11] J. H. Bardarson, F. Pollmann, and J. E. Moore, *Phys. Rev. Lett.* **109**, 017202 (2012); R. Singh, J. H. Bardarson, F. Pollmann, *New J. Phys.* **18**, 023046 (2016); G. De Tomasi, S. Bera, J. H. Bardarson, F. Pollmann, *Phys. Rev. Lett.* **118**, 016804 (2017).
- [12] P. Jurcevic, B. P. Lanyon, P. Hauke, C. Hempel, P. Zoller, R. Blatt, and C. F. Roos, *Nature* **511**, 202 (2014).
- [13] N. Friis, O. Marty, C. Maier, C. Hempel, M. Holzäpfel, P. Jurcevic, M. B. Plenio, M. Huber, C. Roos, R. Blatt, and B. Lanyon, *Phys. Rev. X* **8**, 021012 (2018).
- [14] A. J. Daley, H. Pichler, J. Schachenmayer, and P. Zoller, *Phys. Rev. Lett.* **109**, 020505 (2012).
- [15] R. Islam, R. Ma, P. M. Preiss, M. E. Tai, A. Lukin, M. Rispoli, and M. Greiner, *Nature* **528**, 77 (2015).
- [16] P. Laurell, A. Scheie, C. J. Mukherjee, M. M. Koza, M. Enderle, Z. Tylczynski, S. Okamoto, R. Coldea, D. A. Tennant, and G. Alvarez, *Phys. Rev. Lett.* **127**, 037201 (2021).
- [17] F. Tacchino, A. Auffèves, M. F. Santos, D. Gerace, *Phys. Rev. Lett.* **120**, 063604 (2018).
- [18] R.-Q. Zhang, Z. Hou, Z. Li, H. Zhu, G.-Y. Xiang, C.-F. Li, and G.-C. Guo, *Phys. Rev. Applied* **16**, 024052 (2021).
- [19] G. García-Pérez, M. A. C. Rossi, B. Sokolov, E.-M. Borelli, and S. Maniscalco, *Phys. Rev. Research* **2**, 023393 (2020).
- [20] A. Barasiński, I. I. Arkhipov, J. Svozilík, *Sci. Rep.* **8**, 15209 (2018).
- [21] H. Cheraghi, S. Mahdavifar, *J. Phys.: Condens. Matter* **30**, 42LT01 (2018); H. Cheraghi, M. Jafar Tafreshi, and S. Mahdavifar, *J. Magn. Magn. Mater.* **497**, 166078 (2020); H. Cheraghi and S. Mahdavifar, *Annalen der Physik* **533**, 2000542 (2021).
- [22] P. Titum, J. T. Iosue, J. R. Garrison, A. V. Gorshkov, and Z.-X. Gong, *Phys. Rev. Lett.* **123**, 115701 (2019).
- [23] Z. Gong and M. Ueda, *Phys. Rev. Lett.* **121**, 250601 (2018).
- [24] K. Singh, C. J. Fujiwara, Z. A. Geiger, E. Q. Simmons, M. Lipatov, A. Cao, P. Dotti, S. V. Rajagopal, R. Senaratne, T. Shimasaki, M. Heyl, A. Eckardt, and D. M. Weld, *Phys. Rev. X* **9**, 041021 (2019).
- [25] V. Alba, F. Heidrich-Meisner, *Phys. Rev. B* **90**, 075144 (2014).
- [26] M. Heyl, *Rep. Prog. Phys.* **81**, 054001 (2018).
- [27] S. Diehl, A. Micheli, A. Kantian, B. Kraus, H. P. Büchler, and P. Zoller, *Nat. Phys.* **4**, 878 (2008); S. Diehl, A. Tomadin, A. Micheli, R. Fazio, and P. Zoller, *Phys. Rev. Lett.* **105**, 015702 (2010).
- [28] U. Mishra, A. Bayat, *Phys. Rev. Lett.* **127**, 080504 (2021).
- [29] B. Zunkovic, M. Heyl, M. Knap, and A. Silva, *Phys. Rev. Lett. Phys. Rev. Lett.* **120**, 130601 (2018).
- [30] B. Zhou, C. Yang, and S. Chen, *Phys. Rev. B* **100**, 184313 (2019).
- [31] P. Wang and Ga. Xianlong, *Phys. Rev. A* **97**, 023627 (2018).
- [32] J. C. Halimeh, V. Zauner-Stauber, *Phys. Rev. B* **96**, 134427 (2017).
- [33] M. Cheneau, P. Barmettler, D. Poletti, M. Endres, P. SchauB, T. Fukuhara, C. Gross, I. Bloch, C. Kollath, S. Kuhr, *Nature* **481**, 484 (2012); M. Gring, M. Kuhnert, T. Langen, T. Kitagawa, B. Rauer, M. Schreitl, I. Mazets, D. A. Smith, E. Demler, and J. Schmiedmayer, *Science* **337**, 1318 (2012); S. Trotzky, Y. A. Chen, A. Flesch, I. P. McCulloch, U. Schollwöck, J. Eisert, I. Bloch, *Nat. Phys.* **8**, 325 (2012); T. Langen, R. Geiger, M. Kuhnert, B. Rauer, J. Schmiedmayer, *Nat. Phys.* **9**, 640 (2013).
- [34] S. Sachdev, *Quantum phase transitions*, (Cambridge University press, 2001), ISBN 9780521514682.
- [35] S. M. Giampaolo, G. Adesso, and F. Illuminati, *Phys. Rev. Lett.* **100**, 197201 (2008).
- [36] K. Najafi and M. A. Rajabpour, *Phys. Rev. B* **96**, 014305 (2017).
- [37] E. Lieb, T. Schultz, D. Mattis, *Z. Phys.* **47**, 631 (1928).
- [38] O. Mandel, M. Greiner, A. Widera, T. Rom, T. W. Hänsch, and I. Bloch, *Nature (London)* **425**, 937 (2003).
- [39] D. Leibfried, R. Blatt, C. Monroe, and D. Wineland, *Rev. Mod. Phys.* **75**, 281 (2003).

- [40] Z.-Y. Sun, S. Liu, H.-L. Huang, D. Zhang, Y.-Y. Wu, J. Xu, B.-F. Zhan, H.-G. Cheng, C.-B. Duan, and B. Wang, *Phys. Rev. A* **90**, 062129 (2014).
- [41] E. Canovi, E. Ercolessi, P. Naldesi, L. Taddia, and D. Vodola, *Phys. Rev. B* **89**, 104303 (2014).
- [42] T. Maślowski and N. Sedlmayr, *Phys. Rev. B* **101**, 014301 (2020).
- [43] G. De Tomasi, S. Bera, J. H. Bardarson, F. Pollmann, *Phys. Rev. Lett.* **118**, 016804 (2017).
- [44] R. Jafari, A. Akbari, *Eur. Phys. Lett.* **111**, 10007 (2015).
- [45] J. Surace, L. Tagliacozzo, and E. Tonni, *Phys. Rev. B* **101**, 241107(R) (2020).
- [46] E. Wybo, M. Knap, F. Pollmann, *Phys. Rev. B* **102**, 064304 (2020).
- [47] S. Maity, S. Bandyopadhyay, S. Bhattacharjee, A. Dutta, *Phys. Rev. B* **101**, 180301 (2020).
- [48] S. De Nicola, A. A. Michailidis, M. Serbyn, *Phys. Rev. Lett.* **126**, 040602 (2021).
- [49] Á. Bócsi, B. Dóra, *Phys. Rev. B* **103**, 085137 (2021).
- [50] U. Mishra, H. Cheraghi, S. Mahdavifar, R. Jafari, and A. Akbari, *Phys. Rev. A* **98**, 052338 (2018).
- [51] S. Haldar, S. Roy, T. Chanda, A. Sen, U. Sen, *Phys. Rev. B* **101**, 224304 (2020).
- [52] P. Calabrese and J. Cardy, *J. Stat. Mech.* (2005) P04010.
- [53] M. Rigol, V. Dunjko, and M. Olshanii, *Nature (London)* **452**, 854 (2008).
- [54] L. D'Alessio, Y. Kafri, A. Polkovnikov, and M. Rigol, *Adv. Phys.* **65**, 239 (2016).
- [55] F. Anza, C. Gogolin, and M. Huber, *Phys. Rev. Lett.* **120**, 150603 (2018).
- [56] E. Iyoda, K. Kaneko, and T. Sagawa, *Phys. Rev. Lett.* **119**, 100601 (2017).
- [57] S. Hill and W. K. Wootters, *Phys. Rev. Lett.* **78**, 5022 (1997); W. K. Wootters, *Phys. Rev. Lett.* **80**, 2245 (1998).
- [58] B. P. Lanyon, M. Barbieri, M. P. Almeida, A. G. White, *Phys. Rev. Lett.* **101**, 200501 (2008).
- [59] S. Mahdavifar, S. Mahdavifar, and R. Jafari, *Phys. Rev. A* **96**, 052303 (2017); Z. Shadman, H. Cheraghi, S. Mahdavifar, *Physica A* **512**, 1128 (2018).
- [60] H. Ollivier and W. H. Zurek, *Phys. Rev. Lett.* **88**, 017901 (2001).
- [61] M. S. Sarandy, *Phys. Rev. A* **80**, 022108 (2009).
- [62] R. Dillenschneider, *Phys. Rev. B* **78**, 224413 (2008).
- [63] H. Cheraghi and S. Mahdavifar, *Phys. Rev. B* **102**, 024304 (2020); H. Cheraghi and S. Mahdavifar, *Sci. Rep.* **10**, 4407 (2020); H. Cheraghi, S. Mahdavifar, H. Johannesson, *Phys. Rev. B* **105**, 024425 (2022).
- [64] C. Ding, *Phys. Rev. B* **102**, 060409 (2020).
- [65] D. M. Kennes, D. Schuricht, C. Karrasch, *Phys. Rev. B* **97**, 184302 (2018).